Substance P-induced activation of presynaptic NK1 receptors suppresses EPSCs via nitric oxide synthesis in the rat insular cortex

Sachie Matsumura
Nihon University Graduate School of Dentistry
Major in Pediatric Dentistry
(Directors: Profs. Tetsuo Shirakawa and Masayuki Kobayashi,
Assist. Profs. Kiyofumi Yamamoto and Hiroki Takei)

Index

This thesis is based on the following article and additional results in terms of the effect of Sar-Met on miniature IPSC (Fig. 5):

Sachie Matsumura, Kiyofumi Yamamoto, Yuka Nakaya, Kazunori O'Hashi, Keisuke Kaneko, Hiroki Takei, Hiromasa Tsuda, Tetsuo Shirakawa, and Masayuki Kobayashi (2020) Presynaptic NK1 receptor activation by substance P suppresses EPSCs via nitric oxide synthesis in the rat insular cortex. Neuroscience 455:151-164.

Abstract

Substance P (SP) regulates inhibitory synaptic transmission mediated by $GABA_A$ receptors in the cerebral cortex; however, SP-mediated regulation of excitatory synaptic transmission remains poorly understood. Whole-cell patch-clamp recordings were performed from pyramidal neurons to examine the effects of SP on excitatory postsynaptic currents (EPSCs) mediated via AMPA receptors in the insular cortex (IC), which is involved in nociceptive information processing. First, EPSCs evoked by minimal electrical stimulation (eEPSCs) including stepwise EPSCs and failure events, were examined. SP dose-dependently suppressed mean eEPSC amplitude, partially due to an increase in the failure rate of eEPSCs. The SP-induced suppression of eEPSCs was accompanied by an increase in the paired-pulse ratio and was inhibited by the preapplication of SR140333, an neurokinin 1 (NK1) receptor antagonist. [Sar^9,$Met(O_2)^{11}$]-substance P, an NK1 receptor-selective agonist, mimicked the effects of SP on eEPSCs and decreased the frequency of miniature EPSCs (mEPSCs) without changing the average mEPSC amplitude. Similar to mEPSCs, the application of Sar-Met decreased the frequency of miniature IPSCs (mIPSCs) without changing their amplitude. Considering that most NK1 receptors in the cerebral cortex are expressed in nitric oxide synthase (NOS)-positive GABAergic neurons, the SP-induced suppressive effect on EPSCs may be mediated by nitric oxide (NO) in this subtype of GABAergic neurons. NO imaging using the fluorescent probe DAX-J2 Red supports this hypothesis: SP increased the fluorescence intensity of DAX-J2 Red in some GABAergic neurons. Furthermore, both L-NAME, an NOS inhibitor, and PTIO, an NO scavenger, diminished the SP-induced suppression of eEPSCs. These results suggest that the activation of presynaptic NK1 receptors contributes to SP-induced eEPSC suppression by activating the NO synthesis pathway in GABAergic neurons.

Introduction

Substance P (SP) is a neuropeptide that consists of 11 amino acids and belongs to the tachykinin peptide family, which also includes neurokinin A and neurokinin B (Nakanishi, 1991). SP-immunopositive neurons, most of which are GABAergic interneurons, are widely distributed in the cerebral cortex (Kaneko et al., 1998), and ~70% of GABAergic cortical interneurons are parvalbumin (PV)-immunopositive (Vruwink et al., 2001). Vruwink et al. (2001) proposed that SP is released by volume transmission. Among the three types of tachykinin receptors, which include the neurokinin 1 (NK1), NK2, and NK3 receptors, NK1 receptors are almost exclusively activated by SP (Nakanishi, 1991). In the cerebral cortex, NK1 receptors are principally expressed in the subtype of GABAergic neurons that are also immunopositive for neuronal nitric oxide synthase (nNOS), neuropeptide Y (NPY), and somatostatin (Kubota et al., 2011). Therefore, SP released from PV-immunopositive neurons is widely distributed and activates GABAergic neurons expressing NK1 receptors.

In addition to the coexpression of nNOS, NPY, and somatostatin with NK1 receptors in this GABAergic neural subtype, a functional relationship between NK1 receptors and nNOS has been demonstrated. Whole-cell patch-clamp studies revealed that SP application (30 nM-1 μM) depolarizes the resting membrane potential in nNOS-immunopositive GABAergic neurons (Dittrich et al., 2012), and this effect is mediated by phosphatidylcholine-specific phospholipase C signaling (Endo et al., 2016). The depolarizing effect of SP is observed under the application of tetrodotoxin and glutamate receptor antagonists, suggesting that SP-induced depolarization is not mediated by changing synaptic inputs. These SP-mediated changes in the intrinsic membrane properties are likely to contribute to an increase in the frequency and amplitude of spontaneous but not miniature inhibitory postsynaptic currents (mIPSCs) recorded from cortical pyramidal neurons (PNs; Stacey et al., 2002).

In addition to mIPSCs, excitatory postsynaptic currents (EPSCs) mediated via glutamatergic AMPA and NMDA receptors are also modulated by SP in PNs of the cerebral cortex. SP increased spontaneous EPSC frequency without changing the amplitude of miniature EPSCs (mEPSCs; Stacey et al., 2002), suggesting that SP facilitates spontaneous spike firing of presynaptic glutamatergic neurons. On the other hand, mEPSCs, which are recorded under the application of tetrodotoxin, a voltage-gated Na^+ channel blocker, are not significantly changed by SP, though SP tends to reduce the frequency of mEPSCs (Stacey et al., 2002). In dissociated primary cortical neuronal cultures, SP increases mEPSC frequency without changing their amplitude (Caioli et al., 2011). The discrepancy between these studies in the SP-induced effect on the frequency of mEPSCs indicates that the role of SP in glutamate release in the cerebral cortex remains an open issue.

The insular cortex (IC) receives nociceptive information from the orofacial structures (Horinuki et al., 2015; Nakamura et al., 2015; Horinuki et al., 2016; Nakamura et al., 2016; Kobayashi and Horinuki, 2017; Noma et al., 2019; Zama et al., 2019) and is considered to regulate nociceptive information processing via projections to the limbic structures, including

the amygdala, hypothalamus, and infralimbic cortex (Allen et al., 1991), and descending projections to the medullary dorsal horn (Sato et al., 2013; Kobayashi and Nakaya, 2020). Both PV-immunopositive GABAergic neurons, which express NK1 receptors and SP, and somatostatin-immunopositive GABAergic neurons, some of which express NK1 receptors, are abundantly located in the IC (Chen et al., 2010). These findings suggest that SP may modify nociceptive information processing by regulating the neuronal activities of IC projection neurons.

In the present study, whole-cell patch-clamp recordings were performed from PNs in the rat IC and examined how SP changes intrinsic membrane properties and glutamatergic synaptic transmission in the IC. I further examined the involvement of NO synthesis in the SP-induced modulation of EPSCs.

Materials and Methods

Ethical approval

The Institutional Animal Care and Use Committee at Nihon University approved the study protocol, and all experiments were performed according to the National Institutes of Health Guide for the Care and Use of Laboratory Animals. The number of animals used was minimized as well as their suffering.

Brain slice preparations

Brain slice preparations including the IC were prepared as described previously (Yamamoto and Kobayashi, 2018) with minor alterations. Briefly, 110 vesicular GABA transporter (VGAT)-Venus line A transgenic rats (Uematsu et al., 2008) of either sex (postnatal week 3) were decapitated under deep anesthesia with isoflurane (5%). Cerebrocortical blocks were rapidly removed and submerged in ice-cold modified artificial cerebrospinal fluid (ACSF) (in mM: 230 sucrose, 2.5 KCl, 10 $MgSO_4$, 1.25 NaH_2PO_4, 26 $NaHCO_3$, 2.5 $CaCl_2$, and 10 D-glucose) for 3 min. The cortical blocks including the IC were coronally sliced into 350-µm-thick slices using a microslicer (Linearslicer Pro 7, Dosaka EM, Kyoto, Japan). The cortical slices were then incubated at 32°C for 40 min in a submersion-type chamber that contained 50% modified ACSF and 50% normal ACSF (in mM: 126 NaCl, 3 KCl, 2 $MgSO_4$, 1.25 NaH_2PO_4, 26 $NaHCO_3$, 2 $CaCl_2$, and 10 D-glucose). The ACSF was continuously aerated with 95% O_2 and 5% CO_2. Cortical slices were placed in normal ACSF (32°C) for 1 hr and thereafter kept at room temperature until used for recording.

Whole-cell patch-clamp recording

The slices were transferred to a recording chamber perfused with normal ACSF (2.4 ml/min) and performed whole-cell patch-clamp recordings from Venus-negative pyramidal neurons in IC layer V using a fluorescence microscope with Nomarski optics (40 ×, ECLIPSE FN1, Nikon, Tokyo, Japan) and an infrared-sensitive video camera (IR-1000, DAGE-MTI, Michigan City, USA). Membrane potentials and currents were recorded using amplifiers (Multiclamp 700B, Molecular Devices, Sunnyvale, USA), and the data were digitized (Digidata 1440A, Molecular Devices), recorded online, and stored on a computer hard disk using Clampex (pClamp 10, Molecular Devices).

The composition of the internal solution in the pipette was as follows (in mM): 70 potassium gluconate, 70 KCl, 10 *N*-(2-hydroxyethyl)piperazine-*N'*-(2-ethanesulfonic acid) (HEPES), 2 $MgCl_2$, 2 magnesium adenosine triphosphate (ATP), 0.3 sodium guanosine triphosphate (GTP), and 0.5 EGTA. The internal solution had a pH of 7.3 and an osmolarity of 300 mOsm. The liquid junction potential was -9 mV, and in this study, the voltage was not corrected. A Flaming/Brown micropipette puller (P-97, Sutter Instruments, Novato, USA) was used to make borosilicate patch electrodes (2-5 MΩ; OD = 1.5 mm, ID = 1.17 mm, Harvard Apparatus, Cambridge, UK).

The recording temperature was set at 30 ± 1°C. The seal resistance was > 5 GΩ, and the data obtained from electrodes with access resistance of 6-20 MΩ and < 20% change during recordings were analyzed. Before the EPSC/IPSC recordings, pre- and postsynaptic cell subtypes were identified by neural responses to the application of long (300 ms) hyperpolarizing and depolarizing current pulse injections. Both EPSC and IPSC recordings were performed under voltage-clamp conditions (holding potential = -60 mV). The membrane currents and potentials were low-pass filtered at 5-10 kHz and digitized at 20 kHz.

EPSCs evoked by minimal stimulation and miniature EPSCs

A monopolar tungsten electrode (0.1-0.5 MΩ at 1 kHz) inserted in layers II/III of an IC slice preparation was used for minimal stimulation. Whole-cell patch-clamp recording was performed from a PN that was in close proximity to the stimulation electrode. The distance between the recorded neuron and the stimulation electrode was 100-150 μm. The intensity of electrical stimulation was set at the voltage that evoked EPSCs (eEPSCs), including failure events. Paired-pulse stimulation (50 ms interstimulus interval) was applied to obtain the paired-pulse ratio (PPR), which is sensitive to presynaptic changes in neurotransmitter release (Yamanaka et al., 2017; Usui et al., 2019; Liu et al., 2020). The interval of the paired stimulation was set at 15 s.

To examine the effects of SP and NO on EPSCs, the following drugs were dissolved in the perfusate (normal ACSF): DNQX (40 μM; Abcam, Cambridge, UK), L-NAME (200 μM; FujiFilm, Tokyo, Japan), propylamine propylamine NONOate (NONOate; 100 μM; Abcam), PTIO (100 μM; Tokyo Kasei, Tokyo, Japan), [Sar^9,$Met(O_2)^{11}$]-substance P (Sar-Met; 250 nM; Sigma-Aldrich, St. Louis, USA), SP (10 nM-2 μM; Peptide Institute, Ibaraki, Japan), and SR140333 (1 μM; Tocris Bioscience, Ellisville, USA).

mEPSCs were recorded under the application of tetrodotoxin (1 μM; Abcam), a voltage-gated Na^+ channel blocker, and picrotoxin (100 μM; Sigma-Aldrich), a $GABA_A$ receptor antagonist. mIPSCs were recorded under the application of tetrodotoxin (1 μM), DNQX (40 μM), an AMPA receptor antagonist, and D-AP5 (25 μM; Cayman Chemical, Ann Arbor, USA), an NMDA receptor antagonist.

Imaging of NO synthesis

DAX-J2 Red (DAX-J2; AAT Bioquest, Sunnyvale, USA) was used to detect the synthesis of NO in the cells (Huang et al., 2019). Slice preparations were incubated in normal ACSF with 10 μM DAX-J2 at 26-28 °C for 30 min then rinsed with normal ACSF for 60 min. After the slices were transferred to a recording chamber on a confocal microscope (FV-1000, Olympus, Tokyo, Japan), the field of view was set at layer V of the IC by observation with the 4× objective. DAX-J2 was illuminated by a 559 nm laser with a 60× objective, and fluorescence was filtered with a 575-675 nm bandpass filter (Olympus). To identify GABAergic neurons,

Venus fluorescence evoked by a 473 nm laser was imaged in sequential mode. The speed and resolution of laser scanning were set at 23.8 s/frame and 0.41 μm/pixel, respectively, and a Kalman filter was applied twice.

Mostly, 30-60 frames of images were taken under the application of normal ACSF as a control and then 26 frames were imaged under the application of 1 μM SP. NONOate (100 μM), an NO donor, was applied to verify the response of DAX-J2 to NO.

Immunohistochemistry for NK1 receptors

Rats were deeply anesthetized with isoflurane (5%) and perfused with 60 ml 0.01 M phosphate-buffered saline (PBS; pH 7.4) followed by 4% paraformaldehyde in 0.1 M phosphate buffer (PB, pH 7.4). The brain was removed, post-fixed overnight, cryoprotected in 20% sucrose in PBS, frozen, and sectioned coronally with a sliding microtome (Leica Biosystems, Nussloch, Germany) set at 50 μm. Sections including the IC were rinsed in 0.01 M PBS and treated with HISTOVT ONE (Nacalai Tesque, Kyoto, Japan) 70 °C for 20 min. Then, the sections were treated with a blocking solution consisting of 3% goat serum, and 0.3% Triton X-100 in 0.01 M PBS overnight at 4 °C, and then incubated with polyclonal rabbit anti-NK1 polyclonal antibody (1:1000; ENZO Life Sciences, Farmingdale, USA) diluted in 3% goat serum and 0.3% Triton X-100 in 0.01M PBS for 72 h at 4 °C. The sections were washed in 0.01 M PBS. The sections were incubated with Alexa Fluor 647 anti-rabbit IgG (1:200; Thermo Fisher Scientific, Waltham, USA) for 2 h at room temperature. After rinsing in 0.01 M PBS, the sections were then mounted on gelatin-coated slides and coverslipped.

The slices were imaged using a confocal microscope (FV1000, Olympus, Tokyo, Japan) with a 60 ×/0.90 NA water-immersion objective. LD laser 473 and 635 were used to excite Venus and Alexa Fluor 647, respectively. Two scans were averaged with Kalman filtering. The pixel size was set at 1600 × 1600. Three-dimensional reconstruction was performed. The final schematic figures were generated in Adobe Illustrator (ver. CC 2015, Adobe Systems, San Jose, USA).

Data analysis

Clampfit (pClamp 10, Molecular Devices) was used to analyze the firing and eEPSC properties. An evoked EPSC with an amplitude within the range of noise (< 2 SD of the baseline) was regarded as a failure. The EPSC amplitude was obtained from each sweep. The PPR of the 2nd to 1st eEPSC amplitude was measured from the average EPSC trace obtained from 10 consecutive sweeps to avoid large fluctuations in the failure rates of the 1st EPSCs. The failure rate was calculated from 10 consecutive sweeps. mEPSCs were detected using WDETECTA kindly provided by Professor John Huguenard (Stanford University), and the frequency and amplitude were quantitatively analyzed.

Imaging data were analyzed in MATLAB (MathWorks, Natick, USA) using a custom-written code. I applied 2 × 2 pixel binning to each image for noise reduction; next,

lateral motion artifacts were corrected with a nonrigid method of template matching using NoRMcorre (Pnevmatikakis and Giovannucci, 2017). Images were smoothed with a Gaussian filter with a sigma of 0.8 μm to enhance image structures. The fluorescence of DAX-J2 decreased with time due to photobleaching. Therefore, last, I carried out a bleaching correction by subtracting trends that were obtained by linear fitting of fluorescence data from native signal time courses.

To distinguish signals derived from Venus-positive and Venus-negative regions, every pixel was categorized into two groups using Venus images. If the fluorescence of a pixel was higher than the averaged fluorescence of the entire image, it was categorized as Venus-positive; in the opposite case, the pixel was categorized as Venus-negative. To determine the localization of DAX-J2 fluorescence signals, fluorescence from each pixel was allowed to accumulate over time. Then, only the pixels with signal intensities in the top 5% were superimposed on Venus images.

Statistics

The data are presented as the mean ± the standard error of the mean (SEM). Paired *t*-tests or Student's *t*-tests were used for comparisons between the control and drug-treated groups. In the comparison among 3 groups, *t*-tests were used with Bonferroni correction. The Kolmogorov-Smirnov test was used to compare the cumulative curves of the mEPSC/mIPSC interevent interval and amplitude. Fisher's exact test was used to compare the rate of statistically significant increases in DAX-J2 fluorescence in response to SP between Venus-positive and Venus-negative neurons. All statistical analyses were performed using OriginPro 8J (OriginLab, Northampton, USA). $P < 0.05$ was considered significant. In the DAX-J2 imaging experiment, the numbers of cells and slices are expressed as n and N, respectively.

Results

Whole-cell patch-clamp recording was performed to examine the SP-induced effects on PN activities in the IC. VGAT-Venus transgenic rats were used to enable differentiation between glutamatergic and GABAergic neurons, which are Venus-negative and Venus-positive, respectively. PNs in the IC were identified as glutamatergic neurons with pyramidal-shaped somata and apical dendrites extending vertically toward the cortical surface (Koyanagi et al., 2010; Yamamoto et al., 2010; Kobayashi et al., 2012; Koyanagi et al., 2014).

NK1 receptor expression in the IC

It has been reported that NK1 receptors are located in the cerebral cortex, especially in the GABAergic neuron subtype that mostly contain nNOS, NPY, and somatostatin (Vruwink et al., 2001; Kubota et al., 2011; Dittrich et al., 2012). However, the expression pattern of NK1 receptors in the IC is poorly understood; thus, I first performed immunohistochemical analysis of NK1 receptors in layers II/III of the IC using VGAT-Venus transgenic rats (Fig. 1A, B).

Immunohistochemical analysis of NK1 receptors demonstrated that almost all NK1 receptors-immunopositive-like cell bodies were Venus-positive, as shown in Fig. 1B and C (white arrowheads). Several NK1 receptors-immunopositive dendrites (yellow arrows) and presumed axons (yellow arrowheads) arose from NK1 receptors-immunopositive somata (Fig. 1C).

These findings suggest that NK1 receptors are mostly located in GABAergic neuron somata and their neurites, similar to the results of the previous studies described above.

Suppression of evoked EPSCs by SP

Next, I examined the effects of SP on eEPSCs that were evoked by minimal stimulation via the extracellularly placed sharp monopolar tungsten electrode. Paired-pulse stimulation was applied to obtain the PPR, which is sensitive to presynaptic changes in neurotransmitter release (Yamamoto and Kobayashi, 2018).

Minimal stimulation failed to evoke an EPSC 26.5 ± 6.1% of the time in the control (n = 14; Fig. 2A-C). Application of 250 nM SP increased the failure rate to 59.2 ± 7.7% (n = 14, t(13) = 3.889, P = 0.002, paired t-test; Fig. 2C). The mean amplitude of eEPSCs, including failure events, in the control (20.1 ± 5.7 pA, n = 14) was larger than that under SP application (8.6 ± 3.1 pA, n = 14, t(13) = 2.218, P = 0.04, paired t-test; Fig. 2C). The PPR was increased by SP (1.18 ± 0.17 in the control and 1.63 ± 0.21 during SP application, n = 14, t(13) = 2.4, P = 0.032, paired t-test; Fig. 2C). On the other hand, the mean amplitude of eEPSCs, excluding failure events, in the control was comparable to that under SP application (25.4 ± 5.3 pA in the control and 21.3 ± 4.0 pA during SP application, n = 14, t(13) = 1.523, P = 0.15, paired t-test). Application of 40 μM DNQX diminished eEPSCs (data not shown).

These results suggest that SP suppresses eEPSCs in a presynaptic manner, i.e., via a

reduction in glutamate release from presynaptic terminals.

SP-induced suppression of EPSCs is mediated by NK1 receptors

To examine the dose-dependency of SP-induced eEPSC suppression, the concentration of SP was varied from 10 nM to 2 μM. As shown in Fig. 2D, SP dose-dependently suppressed eEPSC amplitude at concentrations in this range.

To determine which tachykinin receptors mediate SP-induced eEPSC suppression, a selective antagonist of NK1 receptors, SR140333, was applied preceding SP (250 nM). Preapplication of SR140333 (1 μM) diminished the effect of SP on eEPSCs, as shown in Fig. 3A and B. The mean amplitude of eEPSCs, including failure events, under the application of SP and SR140333 (10.0 ± 0.6 pA, n = 9) was comparable to that of SR140333 application alone (9.5 ± 0.7 pA, n = 9, t(8) = 0.7526, $P = 0.4733$, paired *t*-test with Bonferroni correction; Fig. 3C), suggesting that SP suppresses eEPSCs via NK1 receptor activation. Application of SR140333 itself had little effect on eEPSCs in comparison to the control (11.7 ± 1.1 pA, n = 9, t(8) = 1.188, $P = 0.269$, paired *t*-test with Bonferroni correction; Fig. 3C).

To confirm this hypothesis, I next examined the effect of an NK1 receptor-selective agonist, Sar-Met, on eEPSCs. The application of Sar-Met (250 nM) increased the failure rate from 22.9 ± 5.7% to 44.3 ± 9.7% (n = 8, t(7) = -2.732, $P = 0.029$, paired *t*-test; Fig. 3F). The mean amplitude of eEPSCs, including failure events, was decreased by Sar-Met application from 16.7 ± 2.4 pA to 12.0 ± 2.6 pA (n = 8, t(7) = 2.675, $P = 0.033$, paired *t*-test; Fig. 3F), and Sar-Met application also caused an increase in the PPR (1.05 ± 0.14 in control and 1.35 ± 0.22% during Sar-Met application, n = 8, t(7) = -2.373, $P = 0.0486$, paired *t*-test; Fig. 3F).

These results suggest that SP suppresses eEPSCs via NK1 receptor activation.

Sar-Met decreases the frequency of miniature EPSCs and miniature IPSCs without changing their amplitude

The findings obtained from eEPSCs suggest the involvement of presynaptic NK1 receptors in SP-induced suppression of glutamatergic synaptic transmission to PNs. To test this hypothesis, we examined the effects of Sar-Met (250 nM) on mEPSCs. mEPSCs were recorded under the application of 1 μM tetrodotoxin, a voltage-gated Na^+ channel blocker, and 100 μM picrotoxin, a $GABA_A$ receptor antagonist (Fig. 4).

The application of Sar-Met increased the interevent interval of mEPSCs from 0.7 ± 0.1 s to 1.2 ± 0.2 s (n = 9, t(8) = -2.554, $P = 0.033$, paired *t*-test; Fig. 4). On the other hand, mEPSC amplitude was less affected by Sar-Met (6.0 ± 0.5 pA in control and 6.3 ± 0.5 pA under Sar-Met application; n = 9, t(8) = 1.776, $P = 0.11$, paired *t*-test; Fig. 4C).

The cumulative curves of the interevent interval and amplitude were obtained by summing 100 events per PN (n = 9; Fig. 4B). The cumulative curve of the interevent interval from Sar-Met application was significantly different from that of the control ($P < 0.001$,

Kolmogorov-Smirnov test), whereas the cumulative curve of the amplitude from Sar-Met application was comparable to that of the control (P = 0.40, Kolmogorov-Smirnov test; Fig. 4B).

mIPSCs were also recorded under the application of 1 μM tetrodotoxin, 40 μM DNQX, an AMPA receptor antagonist, and 25 μM D-AP5, an NMDA receptor antagonist (Fig. 5). Similar to mEPSCs, the application of Sar-Met increased the interevent interval of mIPSCs from 1.5 ± 0.2 s to 2.0 ± 0.3 s (n = 13, t(12) = 2.489, P = 0.028, paired t-test; Fig. 5). On the other hand, mIPSC amplitude was less affected by Sar-Met (18.8 ± 1.1 pA in control and 17.4 ± 1.1 pA under Sar-Met application; n = 13, t(12) = 1.810, P = 0.09, paired t-test; Fig. 5C).

The cumulative curves of the interevent interval and amplitude of mIPSCs were obtained by summing 100 events per PN (n = 13; Fig. 5B). The cumulative curve of the interevent interval from Sar-Met application was significantly different from that of the control (P < 0.001, Kolmogorov-Smirnov test), whereas the cumulative curve of the amplitude from Sar-Met application was comparable to that of the control (P = 0.22, Kolmogorov-Smirnov test; Fig. 5B).

These results support the above hypothesis that presynaptic NK1 receptor activation decreases both glutamate and GABA release to PNs.

Insignificant changes in the spike firing properties of pyramidal neurons by Sar-Met

Stacey et al. (2002) demonstrated that SP increases the spontaneous EPSC frequency of PNs in the entorhinal cortex, which is likely mediated by SP-induced depolarization of the resting membrane potentials of excitatory presynaptic neurons. To determine whether this finding is also the case of PNs in the IC, their intrinsic membrane and spike firing properties were compared under the current-clamp condition in the control and under the application of 250 nM Sar-Met.

PNs in the IC were identified by detecting pyramidal-shaped somata using Nomarski optics and by detecting cells lacking Venus-positive fluorescence. The resting membrane potential of PNs was -65.3 ± 1.1 mV in the control, and bath application of Sar-Met had little effect on the resting membrane potential (-65.7 ± 1.3 mV, n = 10, t(9) = -0.294, P = 0.78, paired t-test; Fig. 6). Similarly, Sar-Met had a minimal effect on input resistance, which was 125.7 ± 9.2 MΩ in the control and 143.0 ± 15.0 MΩ under the application of Sar-Met (n = 10, t(9) = -1.554, P = 0.16, paired t-test).

To examine spike firing properties, I recorded voltage responses to long depolarizing current pulses that were intracellularly injected (Fig. 6A). The relationship between current intensity and spike firing frequency is shown in Fig. 6B. At all values of injected current intensity evaluated, there was no significant difference in spike frequency (n = 7, t(6) = 0.079-1.925, P = 0.10-0.94, paired t-test).

These results suggest that activation of NK1 receptors has little effect on the intrinsic and spike firing properties of PNs.

SP-induced NO synthesis in GABAergic neurons of the IC

In the cerebral cortex, NK1 receptors are mostly expressed in the GABAergic interneuron subtype composed of cells that predominantly express NOS (Vruwink et al., 2001; Dittrich et al., 2012). In addition, these NOS-immunopositive neurons exhibit SP-induced depolarization of their resting membrane potentials and spontaneous spike firing (Endo et al., 2016). Therefore, SP may promote NO synthesis, especially in some GABAergic neurons. To examine this possibility, NO imaging using DAX-J2, an NO sensor, was performed in neurons of IC slice preparations. Application of SP at 250 nM, the same concentration as the most patch-clamp experiments in this study, increased the optical signals whose onset was obscure with a large variation of the increment in the optical signal amplitude. Therefore, in the following optical imaging experiment, I examined the effect of SP at 1 μM, which induced about 80% reduction of the EPSC amplitude (Fig. 2D).

Bath application of SP (1 μM) to DAX-J2-loaded slice preparations increased the fluorescence of DAX-J2 in the entire field (N = 10, t(9) = 2.904-3.363, $P < 0.001$, paired *t*-test with FDR correction; Fig. 7A and B). To determine which cell subtypes responded to SP, the field was separated into Venus-positive and Venus-negative regions (see Experimental procedures; Fig. 7C). The Venus-positive regions showed a larger increase in the fluorescence induced by SP than the Venus-negative regions (N = 10, t(9) = 2.433-3.648, $P < 0.05$, paired *t*-test with FDR correction; Fig. 7D), suggesting that GABAergic neurons are more sensitive to SP in terms of NO synthesis than other cell types, including glutamatergic excitatory neurons.

I further analyzed the regions that showed an increase in DAX-J2 fluorescence in a different way. The top 5% of regions exhibiting the greatest increase in NO synthesis in response to SP were plotted on the Venus fluorescence images, and the numbers of somata of Venus-positive and Venus-negative cells with and without an increase in DAX-J2 fluorescence were counted (see Experimental procedures). Two examples of IC slices are shown in Fig. 7E-H. Overall, 31.8% of Venus-positive (74/233 obtained from 10 slice preparations) and 20.5% of Venus-negative somata (115/562) showed an increase in DAX-J2 signal ($P < 0.001$, Fisher's exact test). In addition to the fluorescence in the somata, spatially limited fluorescent puncta were scattered in the IC (Fig. 7F and H). The puncta likely correspond to GABAergic axon terminals and/or dendrites because some of the signals overlapped with the Venus fluorescence.

These results suggest that SP promotes NO synthesis principally in a subtype of GABAergic neurons and neurites, including axon terminals.

Inhibition of NO synthesis blocks SP-induced suppression of EPSCs

Taking into account that SP induced NO synthesis in IC, EPSC suppression by SP may be mediated by NO. To explore this possibility, the effect of SP on evoked EPSCs was examined under the blockade of NOS activation.

The NOS inhibitor L-NAME (200 μM) was applied for > 15 min preceding SP application. The coapplication of L-NAME with SP (250 nM) did not change the failure rate (46.1 ± 17.1% under L-NAME application and 38.6 ± 15.5% under coapplication of L-NAME and SP; n = 9, t(8) = 0.767, P = 0.47, paired t-test) or the mean amplitude of the 1st eEPSCs (15.4 ± 3.0 pA under L-NAME application and 18.5 ± 5.2 pA under coapplication of L-NAME and SP; n = 9, t(8) = -0.674, P = 0.52, paired t-test; Fig. 8A-C). The PPR was also not affected by SP in combination with L-NAME (1.54 ± 0.24 under L -NAME application and 1.23 ± 0.26 under coapplication of L-NAME and SP; n = 9, t(8) = 2.063, P = 0.07, paired t-test).

These results suggest that NOS activation is required to induce eEPSC suppression by SP.

Scavenging NO blocks SP-induced suppression of EPSCs

To confirm the contribution of NO to SP-induced suppression of EPSCs, the NO scavenger PTIO was applied in combination with SP.

PTIO (100 μM) was applied for 20 min preceding SP application. The coapplication of PTIO with SP (250 nM) did not change the failure rate (41.8 ± 8.3% under PTIO application and 38.1 ± 6.2% under the coapplication of PTIO and SP; n = 13, t(12) = 0.6577, P = 0.52, paired t-test; Fig. 8D-F) or the mean amplitude of the 1st eEPSCs (12.5 ± 4.1 pA under PTIO application and 15.2 ± 4.0 pA under the coapplication of PTIO and SP; n = 13, t(12) = -1.423, P = 0.18, paired t-test). The PPR was also not affected by SP in combination with PTIO (1.62 ± 0.29 under PTIO application and 1.30 ± 0.29 under the coapplication of PTIO and SP; n = 13, t(12) = 1.780, P = 0.10, paired t-test). Application of PTIO itself had little effect on eEPSCs in comparison to the control (10.9 ± 2.4 pA, n = 13, t(12) = 0.7173, P = 0.49, paired t-test with Bonferroni correction; Fig. 8F).

These results suggest that SP-induced suppression of EPSCs is mediated by NO.

Discussion

The present study examined how SP modulates excitatory synaptic transmission mediated via glutamatergic receptors expressed in the PNs of the IC. I found that bath application of SP dose-dependently suppressed the amplitude of EPSCs evoked by minimal stimulation and increased the failure rate and PPR. These effects were blocked by SR140333 and mimicked by Sar-Met, and Sar-Met decreased the frequency of mEPSCs without changing their mean amplitude. In addition, SP promoted NO synthesis, especially in the GABAergic neuron subtype, and SP-induced suppression of eEPSC amplitude was blocked by L -NAME and PTIO.

SP suppresses glutamatergic synaptic transmission via presynaptic NK1 receptors

The present study suggests that SP reduces glutamate release from presynaptic glutamatergic terminals via NK1 receptors. This hypothesis contradicts the previous study in cultured neurons obtained from the murine cerebral cortex; in this study, SP (200 nM) increased the frequency of mEPSCs without changing their amplitude (Caioli et al., 2011). Stacey et al. (2002) also demonstrated that SP (500 nM) slightly but insignificantly decreased the frequency of mEPSCs in the rat entorhinal cortex without affecting their amplitude. Differences among the local circuits of the IC, cultured cortical circuits, and the entorhinal circuit may have contributed to the discrepancies observed in the effect of SP on EPSCs. First, cultured cortical neurons cannot construct intrinsic local cortical circuits, even though the culture preparation may be suitable for examining neural membrane properties. Second, the layered organization of the entorhinal cortex is distinct from that of the IC; the entorhinal cortex contains three layers, whereas the IC contains five or six layers.

In brain regions other than the cerebral cortex, SP exhibited a variety of effects on glutamatergic synaptic transmission. For example, medium spiny neurons in the nucleus accumbens show SP-induced suppression of EPSCs that is mediated by dopaminergic and purinergic receptors (Kombian et al., 2003; Kombian et al., 2009, 2012). SP-induced suppression of EPSCs has also been reported in the CA1 (Kouznetsova and Nistri, 1998), parabrachial nucleus (Saleh et al., 1996), and nucleus tractus solitarii (Sekizawa et al., 2003). In contrast, SP-induced enhancement of EPSCs has been reported in the CA2 (Dasgupta et al., 2017), lateral posterior nucleus (Masterson et al., 2010), rostral ventromedial medulla (Zhang and Hammond, 2009), and dorsal raphe nucleus (Liu et al., 2002). The results of reduced events in mIPSC supported the idea that NO modulates presynaptic release machinery. However, little information is available about the interaction of SP with NO in glutamatergic synapses. From this point of view, the present findings extend our knowledge of the physiological functions of SP by identifying a possible underlying mechanism.

Localization of NK1 receptors

It has been reported that ascending SP-containing axonal projections arise from the laterodorsal tegmentum and extend toward the medial frontal cortex (Sakanaka et al., 1983; Vincent et al., 1983), possibly including the IC. Furthermore, the principal source of SP in the cerebral cortex is reported to be GABAergic neurons (Penny et al., 1986). Among cortical GABAergic neurons, ~70% of SP-immunopositive neurons express PV, and approximately half of PV neurons are SP-immunopositive (Vruwink et al., 2001). The IC contains an abundance of PV-immunopositive neurons (Chen et al., 2010; Koyanagi et al., 2010), implying a functional significance of SP in information processing in the IC.

Kubota et al. (2011) demonstrated that in the cerebral cortex, some GABAergic neurons that are immunopositive for nNOS, NPY, and somatostatin express NK1 receptors. The present result showing the colocalization of NK1 receptors with VGAT is in agreement with the results of previous studies: NK1 receptors are principally located in a subset of GABAergic neurons but not in PNs. This histochemical finding aligns with the electrophysiological result that Sar-Met did not affect the resting membrane potential or spike firing properties of PNs. Therefore, it is likely that presynaptic rather than postsynaptic NK1 receptors contribute to the changes observed in the electrophysiological properties of PNs, as described below.

SP-induced EPSC suppression is mediated by NOS activation

Cortical GABAergic neurons expressing NK1 receptors respond to SP, which depolarizes the resting membrane potential and partially induces spontaneous spike firing (Stacey et al., 2002; Dittrich et al., 2012; Endo et al., 2016). Endo et al. (2016) have demonstrated that SP-induced depolarization of the resting membrane potential is mediated by the activation of transient receptor potential-like Ca^{2+}-permeable nonselective cation channels via a phosphatidylcholine-specific phospholipase C signaling pathway. This response increases $[Ca^{2+}]_i$, which activates nNOS, and as a result, NO is generated in these neurons. NADPH, a coenzyme collaborating with nNOS, is located in axons (Higo et al., 2009), suggesting that NO is released from GABAergic synaptic terminals. Indeed, NO imaging with DAX-J2 supports this idea: SP promotes NO synthesis in some GABAergic neurons.

NO imaging revealed at least two patterns of DAX-J2 fluorescence in these cells. One was the increased fluorescence in Venus-positive and Venus-negative neuronal somata, and the other was the increased presence of fluorescent puncta around the somata and dendrites (Fig. 7F, H). A subset of the Venus-positive neurons did not show an increase in fluorescence, which agrees with the immunohistochemical finding that most but not all NK1 receptor-expressing GABAergic neurons (Fig. 1C) synthesize NO. Although some Venus-negative somata exhibited increases in DAX-J2 fluorescence, it is possible that fluorescence from the presynaptic terminals on the somata was involved in this phenomenon.

Taking into account the fact that NO can act in a paracrine fashion (Vruwink et al., 2001), NO has a wide variety of transmission pathways, including presynaptic to postsynaptic, postsynaptic to presynaptic, presynaptic to presynaptic, and so on (Kimura et al., 1998;

Burette et al., 2002; Kakegawa and Yuzaki, 2005). Therefore, it is reasonable to postulate that NO triggered by SP-mediated NK1 receptor activation acts on glutamatergic synaptic terminals (Fig. 9). This may be the mechanism by which SP suppresses glutamate release to PNs without NK1 receptor expression in glutamatergic neurons. It cannot be excluded that NO released from the GABAergic neurons may potentiate $GABA_B$ receptors located on the glutamatergic presynaptic terminal (Lopez-Bendito et al., 2002).

The present results of PN suppression presumably via NO release induced by NK1 receptor activation imply that SP changes the excitation-inhibition balance in the IC (Le Roux et al., 2009). Although activities of excitatory cortical neurons are reduced during slow wave sleep, nNOS-immunopositive GABAergic neurons in the cerebral cortex including the IC exhibit higher activities during sleep than the awake period (Kilduff et al., 2011). Therefore, NO synthesis induced by SP-mediated activation of NK1 receptors possibly plays a role in slow wave sleep.

Acknowledgments

The VGAT-Venus transgenic rats were generated by Drs. Y. Yanagawa, M. Hirabayashi, and Y. Kawaguchi of the National Institute for Physiological Sciences, Okazaki, Japan, using pCS2-Venus, which was provided by Dr. A. Miyawaki. I am grateful to Prof. Tetsuo Shirakawa for the opportunity to perform this study, Prof. Masayuki Kobayashi for his instructions of this study, and colleagues in Department of Pharmacology for their technical advice and assistance.

References

Allen GV, Saper CB, Hurley KM, Cechetto DF (1991) Organization of visceral and limbic connections in the insular cortex of the rat. J Comp Neurol 311:1-16.

Burette A, Zabel U, Weinberg RJ, Schmidt HH, Valtschanoff JG (2002) Synaptic localization of nitric oxide synthase and soluble guanylyl cyclase in the hippocampus. J Neurosci 22:8961-8970.

Caioli S, Curcio L, Pieri M, Antonini A, Marolda R, Severini C, Zona C (2011) Substance P receptor activation induces downregulation of the AMPA receptor functionality in cortical neurons from a genetic model of amyotrophic lateral sclerosis. Neurobiol Dis 44:92-101.

Chen S, Fujita S, Koshikawa N, Kobayashi M (2010) Pilocarpine-induced status epilepticus causes acute interneuron loss and hyper-excitatory propagation in rat insular cortex. Neuroscience 166:341-353.

Dasgupta A, Baby N, Krishna K, Hakim M, Wong YP, Behnisch T, Soong TW, Sajikumar S (2017) Substance P induces plasticity and synaptic tagging/capture in rat hippocampal area CA2. Proc Natl Acad Sci USA 114:E8741-E8749.

Dittrich L, Heiss JE, Warrier DR, Perez XA, Quik M, Kilduff TS (2012) Cortical nNOS neurons co-express the NK1 receptor and are depolarized by Substance P in multiple mammalian species. Front Neural Circuits 6:31.

Endo T, Yanagawa Y, Komatsu Y (2016) Substance P Activates Ca^{2+}-permeable nonselective cation channels through a phosphatidylcholine-specific phospholipase C signaling pathway in nNOS-expressing GABAergic neurons in visual cortex. Cereb Cortex 26:669-682.

Higo S, Akashi K, Sakimura K, Tamamaki N (2009) Subtypes of GABAergic neurons project axons in the neocortex. Front Neuroanat 3:25.

Horinuki E, Shinoda M, Shimizu N, Koshikawa N, Kobayashi M (2015) Orthodontic force facilitates cortical responses to periodontal stimulation. J Dent Res 94:1158-1166.

Horinuki E, Yamamoto K, Shimizu N, Koshikawa N, Kobayashi M (2016) Sequential changes in cortical excitation during orthodontic treatment. J Dent Res 95:897-905.

Huang M-Z, Yang Y-J, Liu X-W, Qin Z, Li J-Y (2019) Aspirin eugenol ester attenuates oxidative injury of vascular endothelial cells by regulating NOS and Nrf2 signalling pathways. Br J Pharmacol 176:906-918.

Kakegawa W, Yuzaki M (2005) A mechanism underlying AMPA receptor trafficking during cerebellar long-term potentiation. Proc Natl Acad Sci USA 102:17846-17851.

Kaneko T, Murashima M, Lee T, Mizuno N (1998) Characterization of neocortical non-pyramidal neurons expressing preprotachykinins A and B: a double immunofluorescence study in the rat. Neuroscience 86:765-781.

Kilduff TS, Cauli B, Gerashchenko D (2011) Activation of cortical interneurons during sleep: an anatomical link to homeostatic sleep regulation? Trends Neurosci 34:10-19.

Kimura S, Uchiyama S, Takahashi HE, Shibuki K (1998) cAMP-dependent long-term potentiation of nitric oxide release from cerebellar parallel fibers in rats. J Neurosci 18:8551-8558.

Kobayashi M, Horinuki E (2017) Neural mechanisms of nociception during orthodontic treatment. J Oral Sci 59:167-171.

Kobayashi M, Nakaya Y (2020) Anatomical aspects of corticotrigeminal projections to the medullary dorsal horn. J Oral Sci 62:144-146.

Kobayashi M, Takei H, Yamamoto K, Hatanaka H, Koshikawa N (2012) Kinetics of $GABA_B$ autoreceptor-mediated suppression of GABA release in rat insular cortex. J Neurophysiol 107:1431-1442.

Kombian SB, Ananthalakshmi KV, Parvathy SS, Matowe WC (2003) Substance P depresses excitatory synaptic transmission in the nucleus accumbens through dopaminergic and purinergic mechanisms. J Neurophysiol 89:728-737.

Kombian SB, Ananthalakshmi KV, Zidichouski JA, Saleh TM (2009) Substance P and cocaine employ convergent mechanisms to depress excitatory synaptic transmission in the rat nucleus accumbens in vitro. Eur J Neurosci 29:1579-1587.

Kombian SB, Ananthalakshmi KV, Zidichouski JA, Saleh TM (2012) Cocaine sensitization does not alter SP effects on locomotion or excitatory synaptic transmission in the NAc of rats. Neuropharmacology 62:825-832.

Kouznetsova M, Nistri A (1998) Modulation by substance P of synaptic transmission in the mouse hippocampal slice. Eur J Neurosci 10:3076-3084.

Koyanagi Y, Yamamoto K, Oi Y, Koshikawa N, Kobayashi M (2010) Presynaptic interneuron subtype- and age-dependent modulation of GABAergic synaptic transmission by β-adrenoceptors in rat insular cortex. J Neurophysiol 103:2876-2888.

Koyanagi Y, Oi Y, Yamamoto K, Koshikawa N, Kobayashi M (2014) Fast-spiking cell to pyramidal cell connections are the most sensitive to propofol-induced facilitation of GABAergic currents in rat insular cortex. Anesthesiology 121:68-78.

Kubota Y, Shigematsu N, Karube F, Sekigawa A, Kato S, Yamaguchi N, Hirai Y, Morishima M, Kawaguchi Y (2011) Selective coexpression of multiple chemical markers defines discrete populations of neocortical GABAergic neurons. Cereb Cortex 21:1803-1817.

Le Roux N, Amar M, Moreau AW, Fossier P (2009) Roles of nitric oxide in the homeostatic control of the excitation-inhibition balance in rat visual cortical networks. Neuroscience 163:942-951.

Liu R, Ding Y, Aghajanian GK (2002) Neurokinins activate local glutamatergic inputs to serotonergic neurons of the dorsal raphe nucleus. Neuropsychopharmacology 27:329-340.

Liu Y, Chen QY, Lee JH, Li X-H, Yu S, Zhuo M (2020) Cortical potentiation induced by calcitonin gene-related peptide (CGRP) in the insular cortex of adult mice. Mol Brain 13:36.

López-Bendito G, Shigemoto R, Kulik A, Paulsen O, Fairén A, Luján R (2002) Expression and distribution of metabotropic GABA receptor subtypes $GABA_BR1$ and $GABA_BR2$ during rat neocortical development. Eur J Neurosci 15:1766-1778.

Masterson SP, Li J, Bickford ME (2010) Frequency-dependent release of substance P mediates heterosynaptic potentiation of glutamatergic synaptic responses in the rat visual thalamus. J Neurophysiol 104:1758-1767.

Nakamura H, Shirakawa T, Koshikawa N, Kobayashi M (2016) Distinct excitation to pulpal stimuli between somatosensory and insular cortices. J Dent Res 95:180-187.

Nakamura H, Kato R, Shirakawa T, Koshikawa N, Kobayashi M (2015) Spatiotemporal profiles of dental pulp nociception in rat cerebral cortex: An optical imaging study. J Comp Neurol 523:1162-1174.

Nakanishi S (1991) Mammalian tachykinin receptors. Annu Rev Neurosci 14:123-136.

Noma D, Fujita S, Zama M, Mayahara K, Motoyoshi M, Kobayashi M (2019) Application of oxytocin with low-level laser irradiation suppresses the facilitation of cortical excitability by partial ligation of the infraorbital nerve in rats: An optical imaging study. Brain Res:146588.

Penny GR, Afsharpour S, Kitai ST (1986) Substance P-immunoreactive neurons in the neocortex of the rat: a subset of the glutamic acid decarboxylase-immunoreactive neurons. Neurosci Lett 65:53-59.

Pnevmatikakis EA, Giovannucci A (2017) NoRMCorre: An online algorithm for piecewise rigid motion correction of calcium imaging data. J Neurosci Methods 291:83-94.

Sakanaka M, Shiosaka S, Takatsuki K, Tohyama M (1983) Evidence for the existence of a substance P-containing pathway from the nucleus laterodorsalis tegmenti (Castaldi) to the medial frontal cortex of the rat. Brain Res 259:123-126.

Saleh TM, Kombian SB, Zidichouski JA, Pittman QJ (1996) Peptidergic modulation of synaptic transmission in the parabrachial nucleus in vitro: importance of degradative enzymes in regulating synaptic efficacy. J Neurosci 16:6046-6055.

Sato F, Akhter F, Haque T, Kato T, Takeda R, Nagase Y, Sessle BJ, Yoshida A (2013) Projections from the insular cortex to pain-receptive trigeminal caudal subnucleus (medullary dorsal horn) and other lower brainstem areas in rats. Neuroscience 233:9-27.

Sekizawa S, Joad JP, Bonham AC (2003) Substance P presynaptically depresses the transmission of sensory input to bronchopulmonary neurons in the guinea pig nucleus tractus solitarii. J Physiol 552:547-559.

Stacey AE, Woodhall GL, Jones RS (2002) Neurokinin-receptor-mediated depolarization of cortical neurons elicits an increase in glutamate release at excitatory synapses. Eur J Neurosci 16:1896-1906.

Uematsu M, Hirai Y, Karube F, Ebihara S, Kato M, Abe K, Obata K, Yoshida S, Hirabayashi M, Yanagawa Y, Kawaguchi Y (2008) Quantitative chemical composition of cortical GABAergic neurons revealed in transgenic venus-expressing rats. Cereb Cortex 18:315-330.

Usui M, Kaneko K, Oi Y, Kobayashi M (2019) Orexin facilitates GABAergic IPSCs via postsynaptic OX_1 receptors coupling to the intracellular PKC signalling cascade in the rat cerebral cortex. Neuropharmacology 149:97-112.

Vincent SR, Satoh K, Armstrong DM, Fibiger HC (1983) Substance P in the ascending cholinergic reticular system. Nature 306:688-691.

Vruwink M, Schmidt HH, Weinberg RJ, Burette A (2001) Substance P and nitric oxide signaling in cerebral cortex: anatomical evidence for reciprocal signaling between two classes of interneurons. J Comp Neurol 441:288-301.

Yamamoto K, Kobayashi M (2018) Opposite roles in short-term plasticity for N-type and P/Q-type voltage-dependent calcium channels in GABAergic neuronal connections in the rat cerebral cortex. J Neurosci 38:9814-9828.

Yamamoto K, Koyanagi Y, Koshikawa N, Kobayashi M (2010) Postsynaptic cell type-dependent cholinergic regulation of GABAergic synaptic transmission in rat insular cortex. J Neurophysiol 104:1933-1945.

Yamanaka M, Matsuura T, Pan H, Zhuo M (2017) Calcium-stimulated adenylyl cyclase subtype 1 (AC1) contributes to LTP in the insular cortex of adult mice. Heliyon 3:e00338.

Zama M, Fujita S, Nakaya Y, Tonogi M, Kobayashi M (2019) Preceding administration of minocycline suppresses plastic changes in cortical excitatory propagation in the model rat with partial infraorbital nerve ligation. Front Neurol 10:1150.

Zhang L, Hammond DL (2009) Substance P enhances excitatory synaptic transmission on spinally projecting neurons in the rostral ventromedial medulla after inflammatory injury. J Neurophysiol 102:1139-1151.

Figures

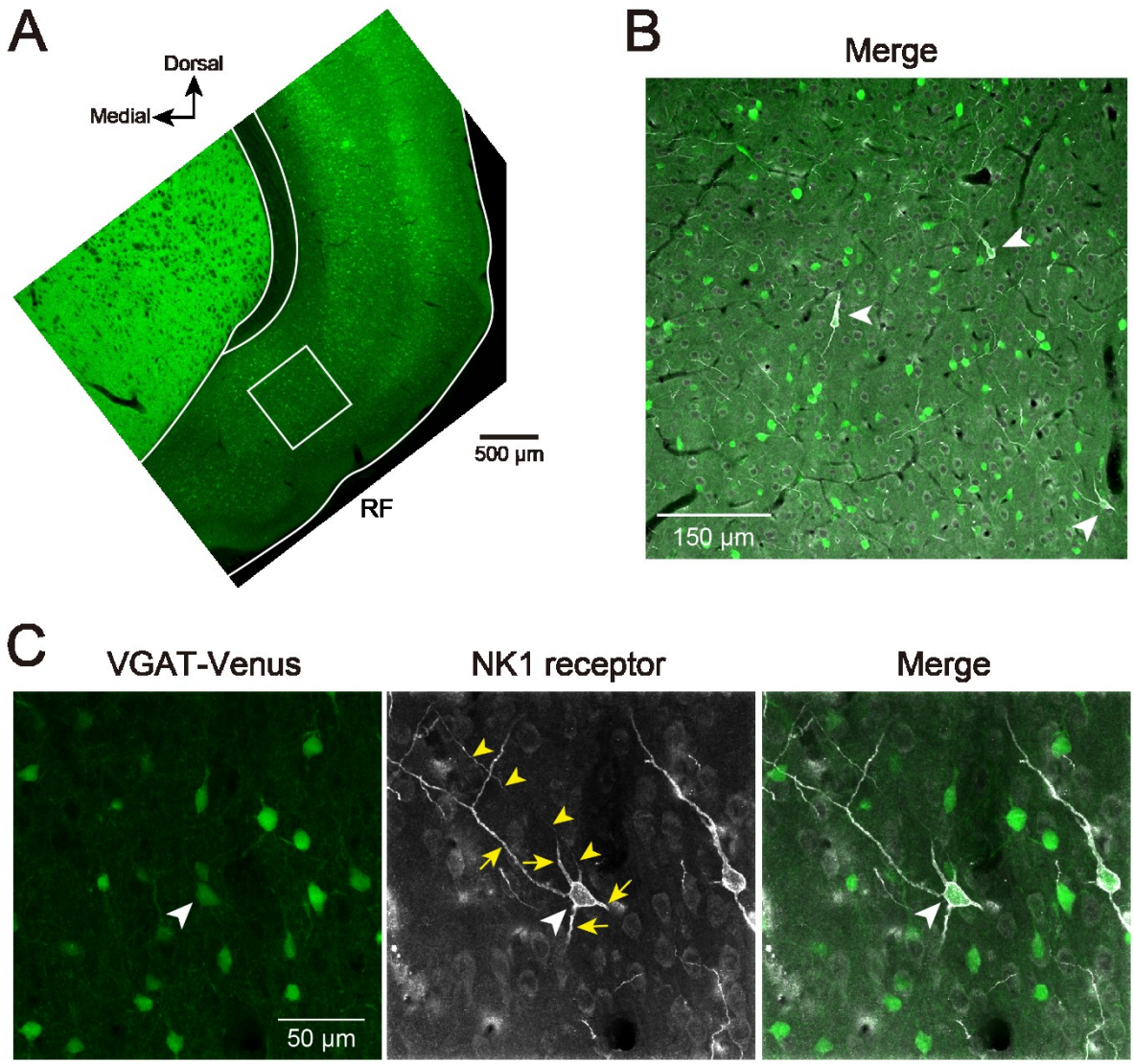

Fig. 1. NK1 receptor expression in the insular cortex (IC). (A) Low-magnification image of the IC and the adjacent cortical region. (B) Expanded image of IC layer V indicated by the box in (A). Arrowheads indicate Venus-positive (green) and NK1-immunopositive (white) neurons. Note that all NK1-immunopositive neurons are Venus-positive (white arrowheads). (C) High-magnification image of the lower neuron indicated by the arrowhead in (B). Three-dimensional reconstruction was performed by overlaying 8 slices that were obtained by changing the focus subsequently at 1.11 μm. Not only the soma (white arrowheads) but also its dendrites (yellow arrows) and presumable axons (yellow arrowheads) are NK1 immunopositive.

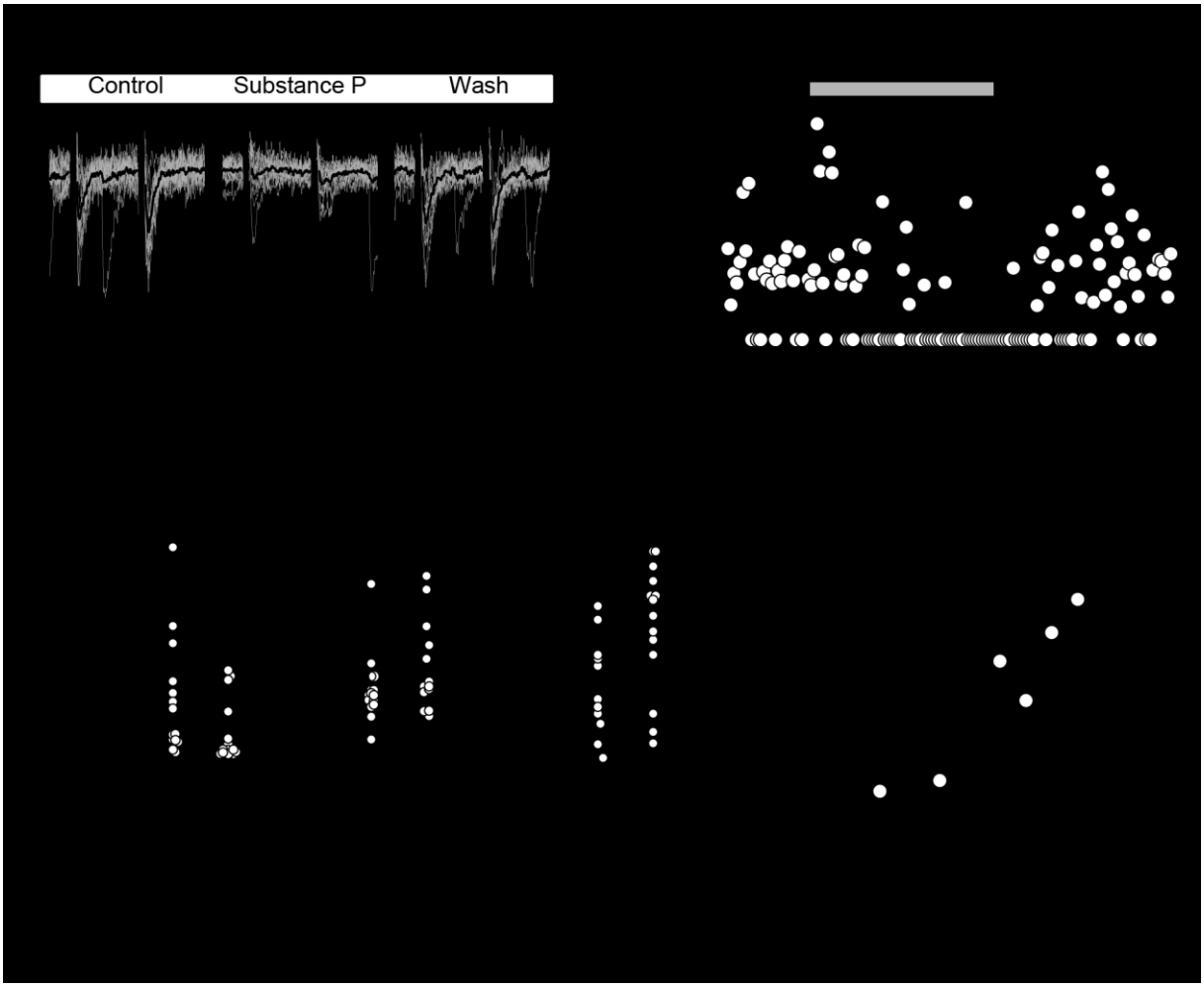

Fig. 2. Substance P (SP; 250 nM) decreases the amplitude of EPSCs evoked by minimal stimulation (eEPSCs). (A) Paired eEPSCs whose interstimulation interval was set at 50 ms. Ten consecutive traces (gray) and their average traces (black) are shown. (B) Time course of the 1st eEPSC amplitude recorded from the PN shown in A. Note the increase in the failure rate of eEPSCs. (C) First eEPSC amplitude (left), the PPR (middle), and the failure rate of the 1st eEPSCs (right) in the control and during SP application (n = 14). Note that SP significantly decreased the 1st eEPSC amplitude and increased the PPR and the 1st eEPSC failure rate. (D) Dose-dependency of SP-induced suppression of eEPSCs. The plots are fitted by the Hill function. The number of neurons is shown in the parentheses. *: $P < 0.05$, paired t-test.

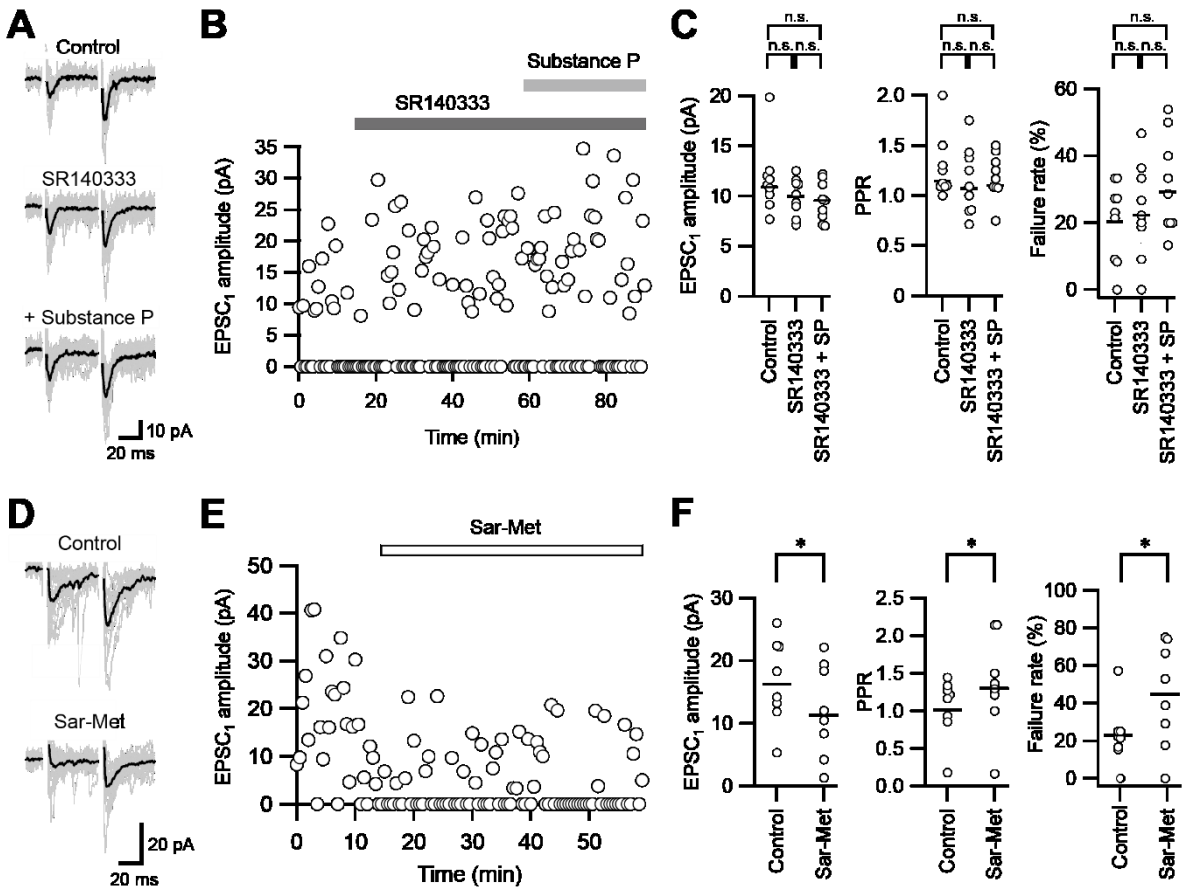

Fig. 3. SP-induced suppression of eEPSCs is likely to be mediated by NK1 receptors. (A) Under the application of 1 μM SR140333, an NK1 receptor antagonist, SP (250 nM) had little effect on eEPSCs. Ten consecutive traces (gray) and their average traces (black) are shown. (B) Time course of the 1st eEPSC amplitude recorded from the PN shown in A. (C) Preapplication of SR140333 diminished the effects of SP on the eEPSC amplitude, PPR, and failure rate. (D) Similar to the effect of SP on eEPSCs, [Sar^9,$Met(O_2)^{11}$]-substance P (250 nM; Sar-Met), an NK1 receptor agonist, decreased the 1st EPSC amplitude. (E) The time course of the 1st eEPSC amplitude recorded from the PN shown in D. (F) Sar-Met mimicked the effects of SP on eEPSCs: a decrease in the 1st eEPSC amplitude and increases in the PPR and the 1st eEPSC failure rate. *: $P < 0.05$, paired t-test.

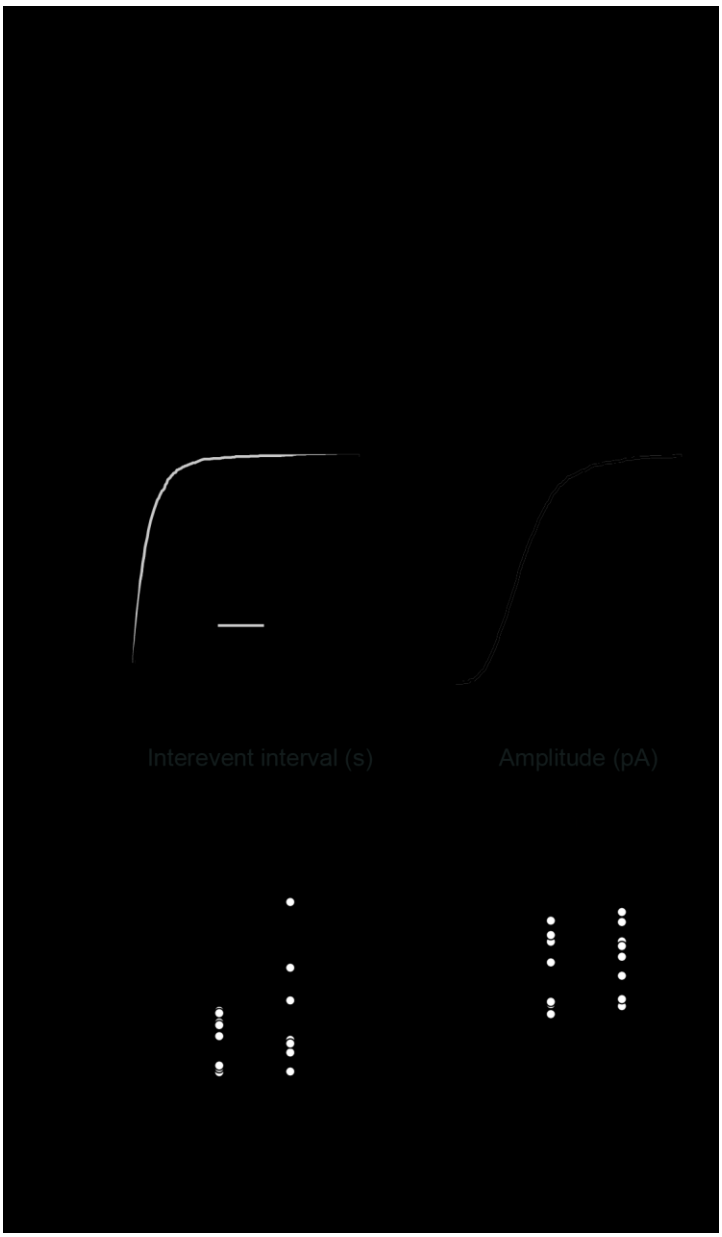

Fig. 4. Sar-Met (250 nM) increases the interevent interval of miniature EPSCs (mEPSCs). (A) Consecutive traces of mEPSCs, which were recorded under the application of picrotoxin (100 μM) and tetrodotoxin (1 μM), in the control (left) and during Sar-Met application (right). (B) Cumulative curves of the interevent interval and amplitude of mEPSCs in the control and during Sar-Met application. Data are summed from 100 events per neuron (n = 9). A significant change was detected in the interevent interval of mEPSCs but not in their amplitude (Kolmogorov-Smirnov test). (C) Sar-Met increased the interval of the mEPSCs without affecting their amplitude. *: $P < 0.05$, paired t-test.

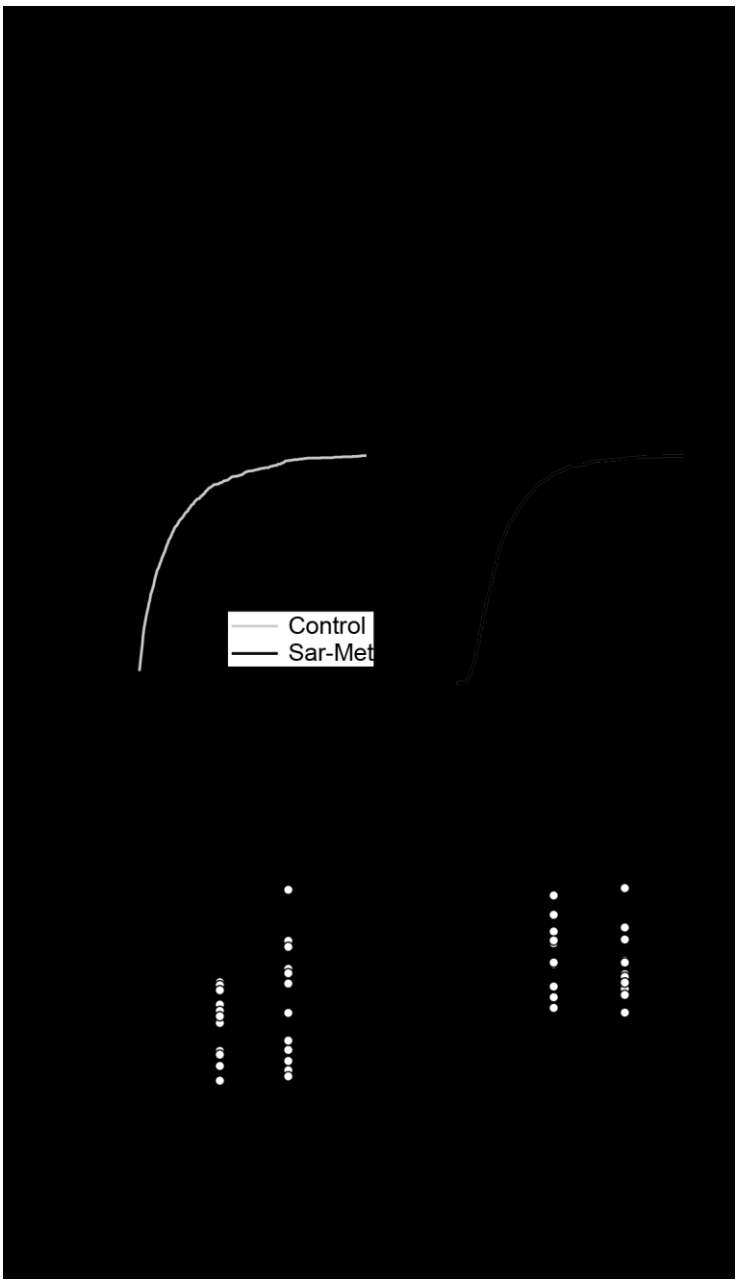

Fig. 5. Sar-Met (250 nM) increases the interevent interval of miniature IPSCs (mIPSCs). (A) Consecutive traces of mIPSCs, which were recorded under the application of DNQX (40 μM), D-AP5 (25 μM), and tetrodotoxin (1 μM), in the control (left) and during Sar-Met application (right). (B) Cumulative curves of the interevent interval and amplitude of mIPSCs in the control and during Sar-Met application. Data are summed from 100 events per neuron (n = 13). A significant change was detected in the interevent interval of mIPSCs but not in their amplitude (Kolmogorov-Smirnov test). (C) Sar-Met increased the interval of the mIPSCs without affecting their amplitude. *: $P < 0.05$, paired *t*-test.

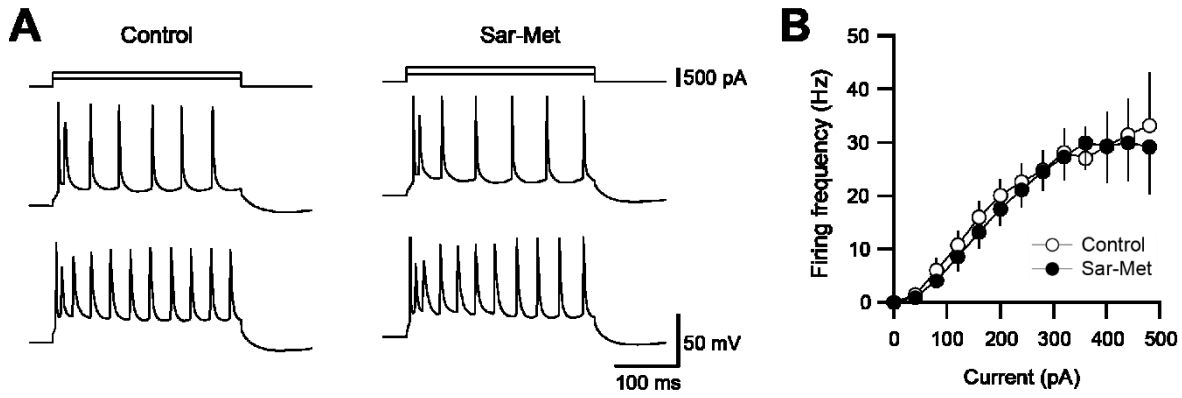

Fig. 6. Effects of Sar-Met (250 nM) on intrinsic membrane properties of pyramidal neurons. (A) Repetitive spike firing properties in the control (left) and during Sar-Met application (right). (B) Relationship between the injected current intensity and firing frequency (f/I curve). Sar-Met had little effect on the f/I curve.

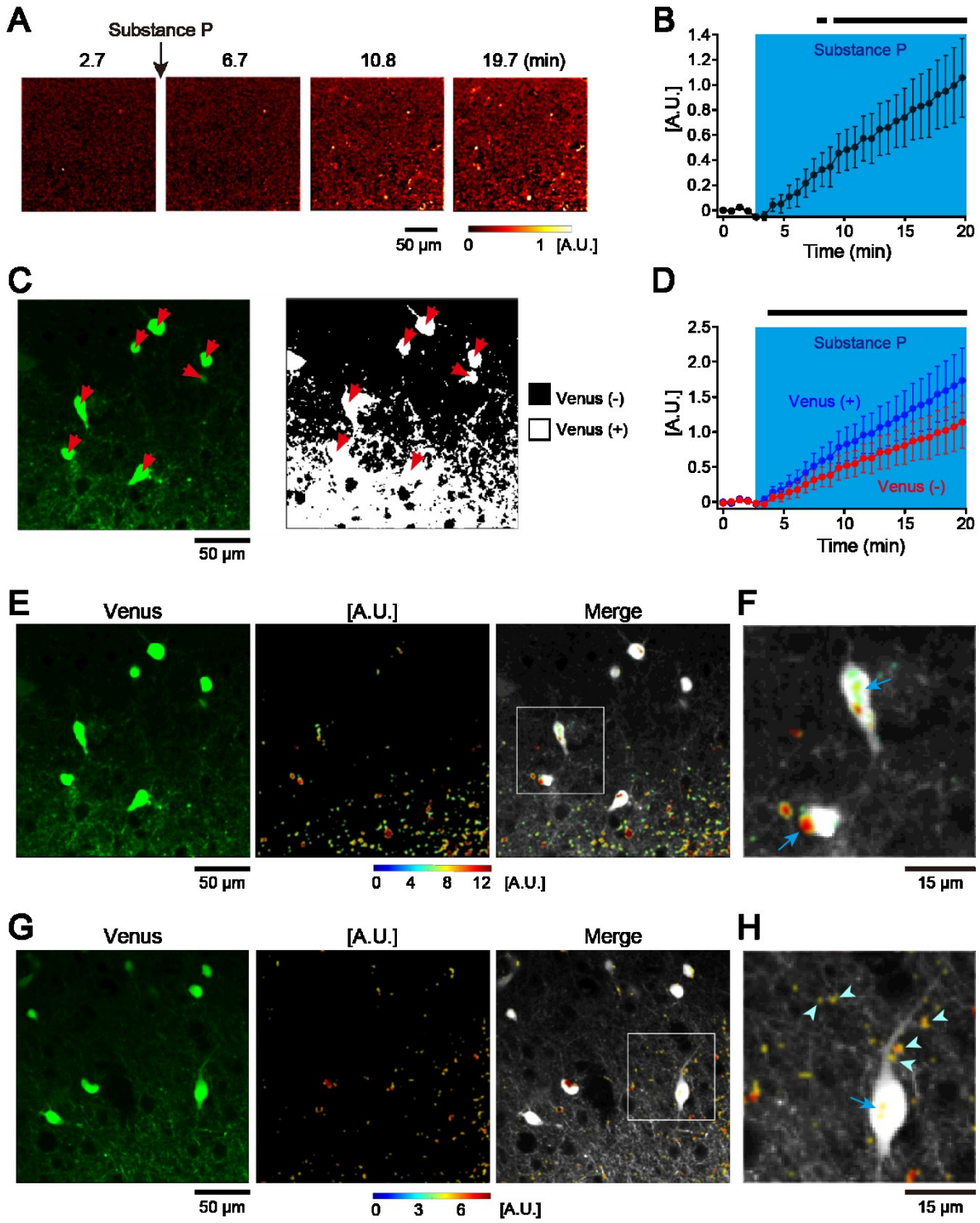

Fig. 7. Effect of SP on NO production. (A) Representative image sequences of DAX-J2 fluorescence patterns with and without SP application. SP was applied just after the first panel (2.7 min). (B) Time-resolved averaged DAX-J2 fluorescence intensities calculated from each entire image with SEM. The SP application period is indicated by a blue shadow. Statistically significant increases (Student's t-test) in DAX-J2 fluorescence intensity by SP application compared to the control (first 4 points) are shown by thick black lines on the top of the graph. (C) An example image of Venus fluorescence. Red arrows indicate Venus-positive somata (left). Mask for Venus-positive (white) and Venus-negative (black) regions (right). If a pixel had a higher fluorescence than the signal averaged over the entire image, it was classified as Venus-positive. On the other hand, a pixel was classified as Venus-negative if its fluorescence was lower than the averaged signal. (D) Time-resolved averaged DAX-J2 fluorescence intensities from Venus-positive (blue) and Venus-negative (red) regions with SEM. Statistical comparisons of fluorescence intensity before and during SP application were performed between

Venus-positive and Venus-negative regions (paired t-test). Statistically significant increases in DAX-J2 fluorescence intensity from SP application in Venus-positive regions compared to Venus-negative regions are shown by thick black lines on the top of the graph. (E) An example of the localization of DAX-J2 fluorescence signals in the top 5% of the detected signal intensities ([A.U.], middle) on Venus fluorescence (left). The merged image is shown in the right panel. (F) An expanded image of the region surrounded by the white rectangle in (E, right). Blue arrows indicate the significant signal increases in DAX-J2 on Venus-positive somata. (G) Another example of localization of DAX-J2 fluorescence signals. (H) An expanded image of the region surrounded by the white rectangle in (G, right). Light blue arrowheads indicate the significant signal increases in DAX-J2 on dendrites.

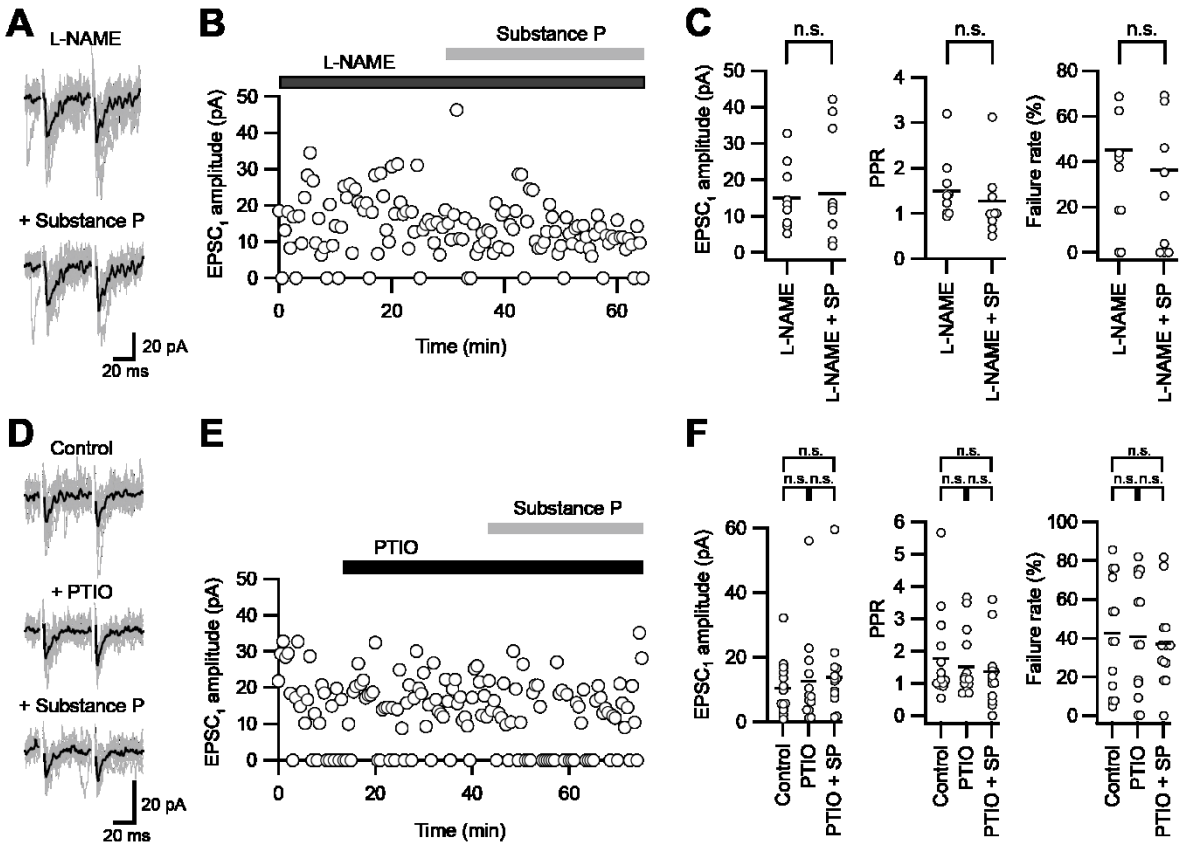

Fig. 8. SP-induced suppression of eEPSCs is likely to be mediated by the activation of nitric oxide synthase (NOS) and the production of nitric oxide (NO). (A) Under the application of 200 μM L-NAME, an NOS inhibitor, SP (250 nM) had little effect on eEPSCs. Ten consecutive traces (gray) and their average traces (black) are shown. (B) Time course of the 1st eEPSC amplitude recorded from the PN shown in A. (C) Preapplication of L-NAME diminished the effects of SP on the eEPSC amplitude, PPR, and failure rate. (D) Under the application of 100 μM PTIO, a scavenger of NO, SP (250 nM) had little effect on eEPSCs. Ten consecutive traces (gray) and their average traces (black) are shown. (E) Time course of the 1st eEPSC amplitude recorded from the PN shown in A. (F) Preapplication of PTIO diminished the effects of SP on the eEPSC amplitude, PPR, and failure rate.

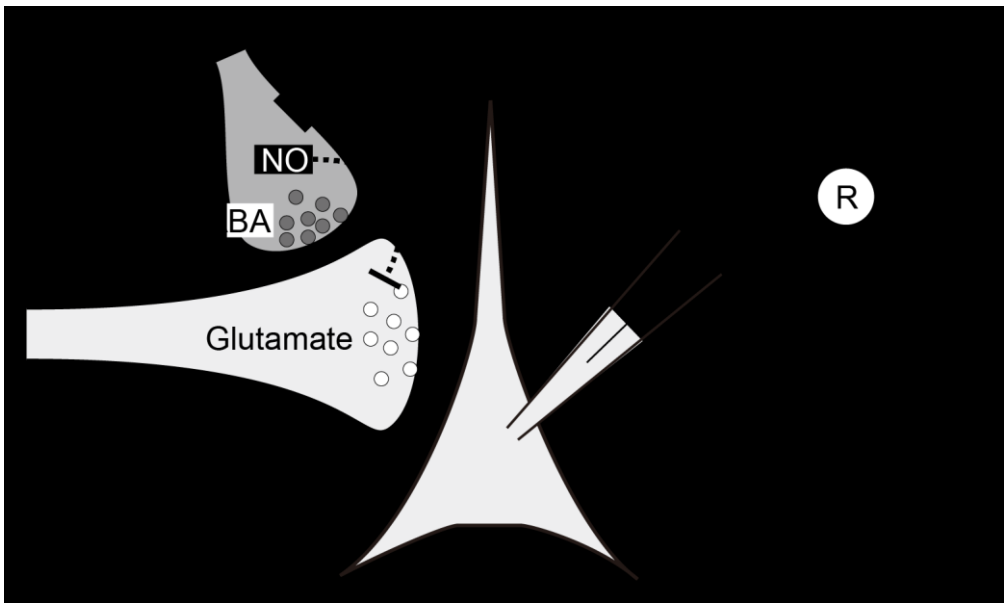

Fig. 9. A possible mechanism of SP-induced suppression of eEPSCs. NK1 receptor activation triggered by SP stimulates NO synthesis principally in GABAergic synaptic terminals, and NO released from presynaptic GABAergic terminals suppresses glutamate release from presynaptic glutamatergic neurons to PNs.